
Article:
Bozon, A., Fries, L., Kammerhofer, J. et al. (4 more authors) (2022) Effect of heterogeneous hydrophobic coating on floating of insoluble particles. Powder Technology, 395. pp. 592-603. ISSN 0032-5910

https://doi.org/10.1016/j.powtec.2021.10.015

Effect of heterogeneous hydrophobic coating on floating of insoluble particles

Annabel Bozon[a], Lennart Fries[b], Jana Kammerhofer[b], Laurent Forny[c], Gerhard Niederreiter[b], Stefan Palzer[d], Agba D. Salman[a]*

[a]Department of Chemical and Biological Engineering, The University of Sheffield, Mappin street, Sheffield, S1 3JD, UK

[b]Nestlé Research, Vers-chez-les-blanc, 1000 Lausanne 26, Switzerland

[c]Nestlé Product Technology Centre, Route de Chavornay 3, 1350 Orbe, Switzerland

[d]Nestlé SA, Avenue Nestlé 55, 1800 Vevey, Switzerland

*Corresponding author: a.d.salman@sheffield.ac.uk

Abstract

Food powders often exhibit hydrophobic surface areas. To understand the effect of corresponding wettability variations on particle floating, which critically influences powder reconstitution, we studied floating of glass beads after creating surface heterogeneity by spraying cocoa butter. Force-position curves were recorded to characterise contact line pinning. Floating of particles with surface heterogeneities comprised a dynamic phase, which to our knowledge has not been reported previously. Measured forces varied due to contact line pinning/depinning. The results indicate that the dynamic floating phase is caused by gradual depinning. Steady-state floating is reached once pinning is sufficiently pronounced.

We also demonstrate that surface heterogeneities complicate theoretical predictions of particle floating. The use of sessile drop contact angles for modelling was identified as an important source of error, as weak pinning points can affect contact angles but are oftentimes overcome during floating. Moreover, local pinning effects are not necessarily represented by a sessile drop.

Keywords: Floating, Particle, Wettability, Surface heterogeneity, Contact line pinning, Force-position curve

1 Introduction

Powdered food products, such as milk powders, infant formula, coffee and malt beverages are of tremendous importance for the food industry. A central quality attribute of these products is a fast and complete reconstitution [1, 2]. However, unsatisfactory reconstitution performance is frequently observed. Floating of powder at the air-liquid interface plays an essential role in this context and is known to be strongly affected by wetting properties [3, 4].

The attachment of bodies to air-liquid interfaces has attracted attention for many years [5-10] and remains an important subject of research until today [11-13]. In the interests of simplification, spheres (rotationally axisymmetric) are commonly used to describe floating phenomena [3, 5, 7, 9, 14-16]. A sphere that is floating at a gas-liquid interface is subjected to downward and upward acting forces. Important parameters are defined in **Figure 1**. The weight or gravitational force F_g (Eq. 1), is the only downward directed force, provided the environment is quiescent [9, 14]. The stabilisation of a sphere at the interface is supported by the buoyancy force F_b (Eq. 2) and the vertical component of the capillary force F_c (Eq. 3) [17]. To enable floating, the weight of the sphere needs to be balanced by F_b and the vertical component of F_c. Floating occurs if F_c is larger or equal than the difference between F_g and F_b, i.e. $F_c \geq F_g - F_b$ [14-16].

$$F_g = V_p \cdot \rho_s \cdot g = \frac{4}{3}\pi R_p^3 \cdot \rho_s \cdot g \quad (1)$$

$$F_b = \frac{\pi R_p^3 \rho_l g}{3}(2 + 3cos\alpha - cos^3\alpha) + \pi(R_p sin\alpha)^2 H \rho_l g \quad (2)$$

$$F_c = 2\pi R_p \gamma sin\alpha \, sin(\theta - \alpha) = 2\pi R_p \gamma sin\alpha \, sin(\beta) \quad (3)$$

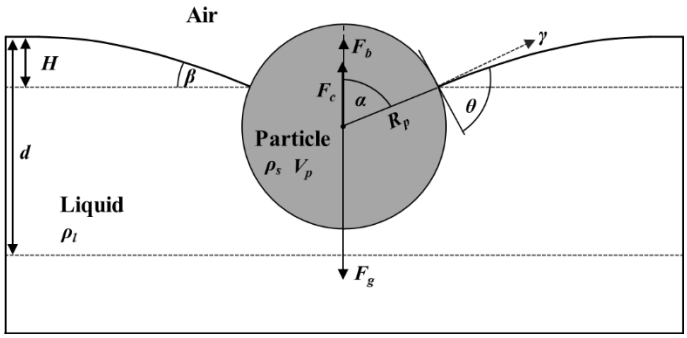

Figure 1: Model representation of a sphere, floating at an air-liquid interface. Indication of gravity force (F_g), buoyancy force (F_b), capillary force (F_c), immersion angle (α), liquid surface tension (γ), liquid density (ρ_l), solid density (ρ_s) contact angle (θ), particle radius (R_p), particle Volume (V_p), immersion depth (d), meniscus depth at the three-phase contact line (H), meniscus slope angle (β).

Force balance analysis is commonly used to predict under which conditions a spherical particle will float [3, 7, 9, 14, 15, 18]. The meniscus depth H at three-phase contact, required for the force analysis can be obtained by solving the Young-Laplace equation of capillary action. The corresponding solution yields the meniscus profile [6, 7, 9, 11, 16, 17, 19]. The validity of theoretical predictions has been verified experimentally. In the scope of this, the importance of surface wettability was pointed out [3, 14, 15]. While it has been demonstrated that capillary forces can aid buoyancy forces and allow spheres to float even if their density is appreciably higher than the liquid density, previous studies focused on model particles with homogeneous surface chemistry, i.e. constant contact angles along the three-phase contact line. The assumption of a constant contact angle in conventional flotation theories has been challenged recently [12, 16]. Considerable contact angle variations along the three-phase contact line, caused by hysteresis, were identified through repeated floating experiments with identical spheres. Based on this, it was concluded that the span of contact angles must be considered for the stability analysis of floating spheres [12]. Yet, until now, the effect of varying surface wettability on particle floating has not been systematically investigated.

Surface heterogeneities are known to affect wetting properties as contact line pinning and deformation can arise if the exerted pinning force is sufficiently strong [20]. The impact of contact line pinning on wetting characteristics, such as contact angles, drop shapes and drop sliding behaviour, has been studied for chemically [21-23] and geometrically [24] patterned surfaces. Varagnolo et al. [23] investigated the sliding behaviour of water droplets on chemically heterogeneous surfaces and demonstrated that pinning-depinning transitions of the contact line affect the type of motion (stick-slip vs. uniform) as well as the sliding velocity. A periodically occurring, large deformation of the three-phase contact line as well as drop velocity fluctuation during vertical droplet sliding across line-patterned hydrophobic surfaces was observed by Suzuki et al. [21]. Jansen et al. [22] observed a corrugated, wave-like contact line due to increased liquid spreading on hydrophilic stripes in comparison to hydrophobic stripes.

Contact angles can also be significantly affected by pinning at sharp edges, known as Gibb's inequality condition [25]. Upon particle immersion, contact lines can remain pinned at sharp edges even if the particle is forced to sink further. As a result of the downward motion (increasing meniscus depth), contact angles and the vertical component of the capillary forces increase [26]. The maximum upward acting capillary force arising during particle immersion is higher for particles with sharp edges in comparison to smooth particles, as experimentally demonstrated by tensiometry [27]. Feng and Nguyen [28] determined acting forces during the immersion of truncated spheres in water and observed that contact line pinning at sharp edges can influence the stability and detachment of floating spheres at air-water interfaces. Ally et al. [29] investigated edge pinning for microscopic particles with defined circumferential cuts using atomic force microscopy.

It has also been shown that surface roughness can cause contact line pinning and impact the forces acting upon particle immersion [27, 29-31]. For instance, pinning of the moving air-water interface has been observed during immersion of spherical particles without apparent sharp edges. Pinning occurred at localised roughness on the particle surface as well as on the

upper particle pole and was sufficient to alter acting forces [31]. It has also been demonstrated that surface roughness influences particle floatability [15, 32, 33], which was explained by the well-known effect of surface roughness on wettability.

The evidenced effect of contact line pinning on contact angles, droplet spreading and forces acting during immersion suggests that particle floating is also affected. Considering that food powders are commonly characterised by irregular shapes, surface roughness, sharp corners and edges as well as by chemically heterogeneous surfaces of alternating wettability [34-36], studying floating at pinning conditions can contribute to a better understanding of the behaviour of commercial food powders at air-liquid interfaces.

Although the attachment of particles to air-liquid interfaces has been studied for many years, floating of particles with chemically heterogeneous surfaces of alternating wettability, as commonly present for food powders, is not understood. As a first step to extend the studies of complex wetting characteristics to the case of a floating sphere, insoluble glass beads were chosen as model particles. The floating behaviour of individual beads was studied after creating surface heterogeneities in the form of distributed hydrophobic coating material (partial coating) and as defects in a coating shell.

2 Material and methods

2.1 Material

Glass beads (Retsch GmbH, Germany), in the following referred to as GB, were used as core material. The beads possess a d_{50} value of 678 µm (d_{10}: 567 µm, d_{90}: 791 µm) and sphericity of 0.94, as determined with a particle size analyser (Camsizer, Retsch Technology, Germany). Cocoa butter (Olam International, Singapore) was used as a coating material to modify surface hydrophobicity. Large glass beads (R_p = 2453 ± 53 µm, microscopically determined, VHX-

5000, Keyence Corporation, Japan) were used to generate model particles with a defined coating pattern (Section 2.11).

2.2 Pretreatment of glass beads

GB were cleaned by sequential immersion in Ethanol (99% absolute, Fisher Chemical, UK) and deionised water in an ultrasonic bath for 15 min, repeated three times. The beads were recovered by sieving, rigorously rinsed with deionised water and dried in an oven at 70°C. A part of the cleaned beads was stored for 1.5 h in HCl (1 Mol/L, Fluka Analytical, Switzerland) to eliminate contaminants and thus increase surface hydrophilicity. Following decantation, the reaction was stopped by washing with deionised water and the beads were dried in an oven at 70°C for 4 h. The treated beads are referred to as HGB (hydrophilic glass beads). Hydrophilic surface treatment, coating and analysis of wettability and floating were conducted within one day to minimise the risk of re-contamination and hence alteration of surface hydrophilicity.

2.3 Surface coating of glass beads

GB were coated with cocoa butter using a top-spray fluidized bed coater (Glatt GPCG3, Glatt GmbH, Germany). Molten cocoa butter (about 75°C) was sprayed with a two-fluid nozzle (flow rate: 1.27 g/min; atomizing air pressure: 1.5 bar) on fluidized particles (50 g beads, fluidizing air temperature: 20 ± 5°C). Spraying time was adjusted (1.2 – 4.4 min) to produce four coated glass bead (CGB) samples (CGB1 – CGB4) of varying surface characteristics in terms of coating quantity and distribution. To inhibit premature solidification of cocoa butter, spray nozzle and atomizing air were heated with an electrical heater to 60 – 70°C and 80°C, respectively. After spraying, fluidization was continued for 10 min at 20 ± 5°C fluidizing air temperature to initiate cocoa butter solidification. Samples were then spread out as a layer and stored at ambient temperature overnight. Agglomerated by-products were removed by sieving

with a 1000 µm sieve at an amplitude of 1.5 mm for 1 min using a sieve shaker (Retsch AS 200 control, Retsch GmbH, Germany).

2.4 Surface coating of hydrophilic glass beads

Hydrophilic glass beads (HGB) were used as core material to produce a coated sample (CHGB) with increased wettability contrast. Coating was conducted by mixing 10 g HGB with 0.03 g cocoa butter powder. This approach was chosen to reduce processing and exposure time to the environment (during fluidization), as both factors facilitate re-contamination. HGB and cocoa butter powder (≤ 300 µm, stored at 4°± 2ºC) were directly weighted in a glass vial. The vial was tightly closed, turned over several times and placed in an oven at 70°C for 30 min to induce cocoa butter melting. Afterwards, cocoa butter was distributed by turning the vials over several times. Storage at 70°C for 30 min and subsequent mixing was repeated once more to allow even spreading of molten cocoa butter. The coated sample was cooled to ambient temperature, sealed and stored at 4 ± 2ºC for 30 min to ensure complete cocoa butter solidification.

2.5 Assessment of coating quantity by solvent extraction

The actual coating quantity was determined by solvent extraction. For this purpose, 2 ± 0.01 g powdered sample was weighted in a glass bottle and 40 ml extractant (99% n-heptane, Sigma Aldrich, USA) was added. The bottles were closed, and shaking was executed with an automatic shaker (PSU-20i, Grant Instruments, UK) at 90 strokes/min for 1 h. Suspensions were left at ambient temperature overnight. The extract was filtered (Folded filter paper, Whatman, type 595 ½, 4 – 7 µm, GE Healthcare Life Sciences, UK Limited) and 25 ml of the filtrate were pipetted in a pre-weighed aluminium dish (200 ml, 65 mm, Fisherbrand, UK). The dishes were placed on a heating plate at 102 ± 5°C to evaporate the solvent. To avoid losses of cocoa butter, boiling of the extract was prevented by removing the dishes regularly from the heating plate. After evaporation, the dishes were cooled to ambient temperature in a desiccator (filled with

silica gel) for at least 20 min. The dishes were weighted and the mass fraction of cocoa butter in g per 100 g sample was calculated. Sample mass and solvent quantity were halved for sample CHGB. Analysis was conducted in triplicate.

2.6 Assessment of surface coverage by light microscopy

The distribution of coating material on the bead surface was assessed by light microscopy (VHX-5000, Keyence Corporation, Japan). Images of 20 individual particles of each sample were recorded at 200 x magnification from frontal view using a 90° tilted microscope lens.

2.7 Contact angle measurement by sessile drop technique

Contact angles with water were determined by placing sessile drops on the apex of individual particles (contact line cord: 86 ± 19 µm). The wetting process was recorded (15 fps, resolution 1600 (H) x 1200 (V)) at 200 x magnification with a 90° tilted microscope lens (VHX-5000, Keyence Corporation, Japan). Videos were converted to images and the apparent contact angle θ_a was measured relative to the horizon using a contact angle Plugin of ImageJ software (1.51k; Java 1.6). As a result of the sphere curvature, θ_a overestimates the intrinsic contact angle value $\theta_{a,i}$, which would be expected on a flat surface of identical composition [37]. The intrinsic contact angle was therefore calculated using Eq. (4), introduced by Extrand and Moon [37].

$$\theta_{a,i} = \theta_a - sin^{-1}\left(a/R_p\right) \quad (4)$$

Contact line cord ($2a$) and particle radius (R_p) were determined via ImageJ software (1.51k; Java 1.6). Measurements were conducted immediately upon droplet deposition (within 0.07 s) for 10 replicates.

The apparent contact angle of pure cocoa butter was determined on compressed tablets (diameter: 30 mm, height: 17 mm, weight: 7 g), produced at 1 kN compaction pressure and

10 mm/min compaction speed using a material testing system (Instron 3369). To avoid melting, which impaired tablet formation, cocoa butter powder was cooled (4 ± 2ºC) before tabletting. A drop of deionised water was placed on the tablet surface (contact line cord: 1.04 ± 0.4 mm) and the contact angle was measured within 0.1 s using a goniometer (FTA125, First Ten Angstroms, UK). The average contact angle was determined based on 20 replicates. All contact angle measurements were conducted at room temperature.

2.8 Experimental assessment of particle floating

Floating behaviour of individual particles was studied over time. Polystyrene cuvettes (FB55143, Fisherbrand, UK) were filled with 3.5 ml deionised water (ambient temperature) and positioned in front of a 90° tilted microscope lens (VHX-5000, Keyence Corporation, Japan). Individual particles were carefully placed on the centre of the water surface using vacuum tweezers (Dymax 5, Agar Scientific, UK). The floating process was recorded below the waterline with a frame rate of 15 fps at 200 x magnification (resolution 1600 (H) x 1200 (V)). Care was taken to focus on the particle contour in the liquid phase to assure a high measurement accuracy (evade the impact of light refraction). Videos were converted to images to measure particle radius (R_p) and immersion depth (d) using Keyence VHX communication software. For comparability, the percentage of particle immersion, $d\%$ (percentage of particle diameter, immersed in water), was calculated using Eq. (5).

$$d\% = \frac{100 \cdot d}{2 \cdot R_p} \tag{5}$$

Data collection was started 1 s after placing the bead at the interface (to allow time for alignment of the bead) and continued until steady floating (constant $d\%$) was reached. To assess the effect of varying surface coating on floating, experiments were conducted with beads of comparable size (R_p = 350 ± 50 µm). Theoretical calculations (Eqs. 1 – 3, 13, 14) indicate that particle size

variations within this range affect the floating position by a maximum of 1.6%. The used deionised water was replaced after each measurement.

2.9 Measurement of force-position curves by tensiometry

The force acting on individual beads during immersion in water was measured for uncoated GB, HGB and coated CGB1 - CGB4 beads using a force tensiometer (K100, Krüss GmbH, Germany). Beads were attached to a steel rod (0.5 mm diameter) using double-sided adhesive carbon tape. The upper end of the steel rod was clamped to the tensiometer microbalance and the sample was lowered above a glass beaker filled with deionised water (20 ± 1°C). Subsequently, the air-liquid interface was moved over the stationary bead by raising the tensiometer stage (i.e. the beaker) automatically at a constant velocity of 1000 µm/min. The beads were immersed 500 µm into the water phase and the acting force was recorded in increments of 1 µm. A schematic illustration of the experimental setup is depicted in **Figure 2**.

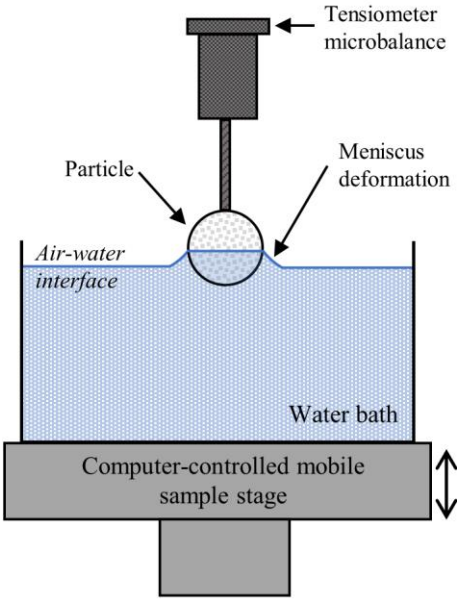

Figure 2: Schematic illustration of the experimental setup to measure force-position curves with a tensiometer. The state of particle immersion, resulting in meniscus deformation (exaggerated for clarity) is shown.

Prior to particle immersion, the microbalance was tared in the air phase. Hence, the gravity force is omitted and the recorded force corresponds to the sum of capillary and buoyancy force. Downward acting forces are defined as positive and upward acting forces as negative in the obtained force-position curve. Ten replicate measurements were conducted for each sample and the data were averaged. The water was changed between every measurement. As acting forces are affected by particle size, tensiometric measurements were conducted with beads of narrow particle radius (350 ± 10 µm) selected from each sample.

2.10 Prediction of acting forces and floating position

The floating position at the air-water interface was predicted based on established models from the literature [3, 6, 9, 17]. The force balance ($F_g + F_c + F_b = 0$), as introduced through Eqs. (1 – 3), was used to calculate the theoretical particle immersion depth expected for uncoated (GB, HGB) and coated (CGB1 – CGB4, CHGB) samples based on underlying liquid (γ, ρ_l) and solid properties (ρ_s, R_p, θ). Solid density, liquid density and surface tension included in Eqs. (1 – 3), were kept constant at 2500 kg/m^3 ($\approx \rho_s$ of glass [38]), 998 kg/m^3, 72.8 mN/m, respectively. The solid density was not adjusted for each sample, as the applied coating quantities are not sufficient to alter the particle density to any extent relevant for floating (see Section 3.2).

Particle sizes, considered for model predictions (Eqs. 1 – 3), were measured during floating. Lastly, experimentally determined contact angles (Section 2.7) were included in the model (Eq. 3). Due to the high impact of wettability on particle floating, predictions were performed for average contact angles and within corresponding 95%-Confidence intervals.

To solve the force balance, the meniscus depth H at three-phase contact must be known (see Eq. 2). The meniscus shape can be described by the Young-Laplace-equation of capillary action [6]. The mean curvature of the deformation is described by the second and first derivatives of

the meniscus depth (h) with respect to the radial coordinate (r) [17]. For the case of the rotationally symmetric sphere, the Young-Laplace equation becomes:

$$\gamma\left\{\frac{d^2h/dr^2}{[1+(dh/dr)^2]^{3/2}}+\frac{dh/dr}{r[1+(dh/dr)^2]^{1/2}}\right\}=\ g(\rho_l-\rho_a)h=0 \qquad (6)$$

$$\frac{dh}{dr}=\ tan\beta \qquad \text{at } r=r_0 \qquad (7)$$

$$\frac{dh}{dr}\rightarrow\ 0 \qquad \text{at } r\rightarrow\infty \qquad (8)$$

where γ is the interfacial tension between air and liquid with density ρ_a and ρ_l and r_0 is the radius of the contact point [6]. Boundary conditions are the meniscus inclination at the contact line (Eq. 7) and the meniscus flatness far away from the contact line (at infinity) (Eq. 8). Already incorporated in Eq. (6) is the additional condition that $h \rightarrow 0$ as $r \rightarrow \infty$ [6]. To describe Eq. (6) as a scaled equation, the meniscus coordinates h and r are divided by the capillary length $L = \sqrt{\gamma/\rho_l g}$ [17]:

$$\frac{d^2y/dx^2}{[1+(dy/dx)^2]^{3/2}}+\frac{dy/dx}{x[1+(dy/dx)^2]^{1/2}}-y=\ 0 \qquad (9)$$

$$\frac{dy}{dx}=\ tan\beta \qquad y=-H/L \qquad \text{at } x=x_0 \qquad (10)$$

$$\frac{dy}{dx}=\ 0 \qquad y=0 \qquad \text{at } x\rightarrow\infty \qquad (11)$$

where $y \equiv \frac{h}{L} = h/\sqrt{\gamma/(\rho_l g)}$, $x \equiv \frac{r}{L} = r/\sqrt{\gamma/(\rho_l g)}$ are dimensionless variables and $x_0 = \left(\frac{R_p}{L}\right) sin\alpha$ is the scaled radius of the three-phase contact. Boundary conditions at the three-phase contact line and far away from the triple line are given by Eqs. (10) and (11), respectively [17].

After replacing boundary conditions to transform the two-point boundary value problem to an initial-value problem, Eq. (9) can be simplified to the following version of the Bessel equation [6]:

$$y(x) = -\frac{K_0(x)}{K_1(r_0/L)} tan\beta \tag{12}$$

where K_0 and K_1 are modified Bessel functions of the second kind and zero and first order. At the triple line: $y = -H/L$; $\frac{dy}{dx} = tan\beta = \tan(\theta - \alpha)$ and $x_0 = \left(\frac{R_p}{L}\right) sin\alpha$ with $r_0 = R_p sin\alpha$ (compare Eq. 10). Hence, to determine H, Eq. (12) can be transformed to:

$$H = -L \tan(\theta - \alpha) \frac{K_0\left(\frac{R_p sin\alpha}{L}\right)}{K_1\left(\frac{R_p sin\alpha}{L}\right)} \tag{13}$$

Solving the force balance ($F_g + F_c + F_b = 0$), using Eqs. (1 – 3) at given γ, ρ_l, ρ_s, R_p, θ, the values for α and H can be derived and the equilibrium floating position of the sphere calculated with Eq. (14) [3].

$$d = R_p(1 + cos\alpha) + H \tag{14}$$

The solution of Eq. 14 is stable if the derivative of the sum of forces with respect to the immersion depth is negative, i.e. if $dF_{net}/d\alpha < 0$. The solution is unstable if $dF_{net}/d\alpha > 0$ holds true [9]. Predicted immersion depths were converted to respective $d\%$ values (Eq. 5) to improve comparability. The three force components were additionally calculated as a function of immersion depth at defined solid and liquid properties.

2.11 Preparation and analysis of model particles with defined coating

Model particles with defined coating were produced with large glass beads (R_p = 2453 ± 53 µm, microscopically determined) and molten cocoa butter. To enhance visibility, cocoa butter was dyed red with 0.05% w/w Ponceau 4R, E124 (MSK Ingredients Ltd., UK). Pretreatment of beads, including storage in HCl, was conducted as described in Section 2.2. Individual beads were attached to steel rods (0.8 mm diameter) using double-sided adhesive carbon tape. In the following, the bead pole opposite the attachment point is referred to as sphere top. The first type of sample, named top-coated, was produced by placing a 1 µl droplet of molten cocoa butter on the sphere top. The second sample type comprised a coating pattern of four separated coating spots. In this case, the sphere top was left uncoated and four 1 µl cocoa butter droplets were uniformly distributed on the top half of the sphere. Dimensions and exact position of each coating spot were determined microscopically. Fully coated samples were prepared by submerging beads 5 mm deep into molten cocoa butter. Beads were turned over immediately upon removal from the cocoa butter bath to inhibit accumulation of coating material at the sphere top.

Coated beads were stored in glass containers overnight to allow time for cocoa butter solidification. The uncoated reference sample was stored in the same manner, to keep the period between HCl treatment and sample analysis identical for all beads. Force-position curves were determined as described in Section 2.9. However, beads were immersed 5 mm at a velocity of 5 mm/min and acting forces were recorded in 0.01 mm increments. For uncoated samples, sessile drop contact angles were measured on individual beads to calculate theoretical force-position curves.

3 Results and discussion

3.1 Analysis of wettability as a function of surface composition

GB and HGB were used as core material of coated samples CGB1 - CGB4 and CHGB, respectively. Microscopic images depicting an exemplary particle of each sample, reflecting the surface coverage are shown in **Figure 3**. Actual cocoa butter quantity, measured by solvent extraction, is given in **Figure 3Table 1**.

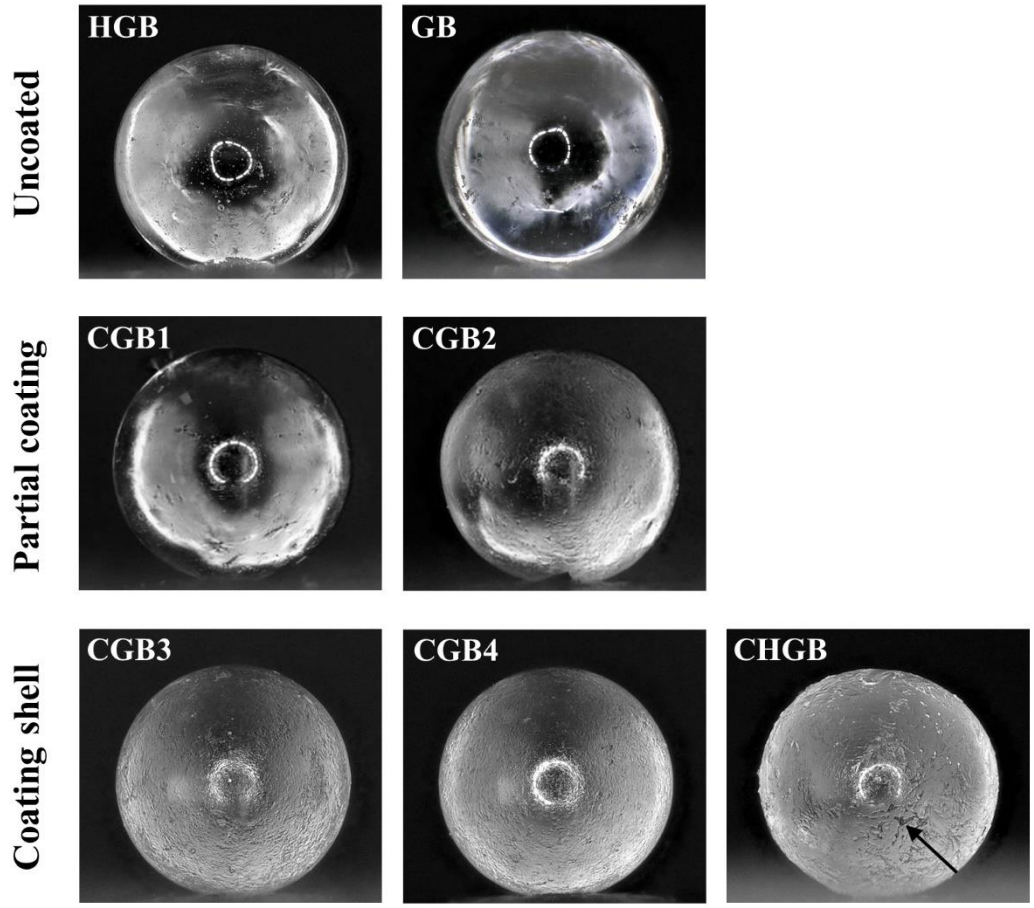

Figure 3: Microscopic images (front view, 200 x magnification) of uncoated beads (HGB, GB), partially coated beads (CGB1, CGB2) and beads comprising a coating shell (CGB3, CGB4, CHGB). Arrow indicates a defect in the coating shell.

Uncoated HGB and GB possess a rather homogeneous polished surface. For sample CGB1 a cocoa butter content of 0.03 ± 0.02% was determined. Considering the measurement accuracy, this sample is classified as < 0.1% coated. No clear difference between particles of sample

CGB1 and the respective core material GB was observed microscopically. The higher coating quantity of sample CGB2 (0.1%) is accompanied by an increase of coated surface area as indicated by the enhanced particle opaqueness. While sample CGB3 exhibits an identical coating quantity (0.1%), microscopic images reveal that the coating is characterised by a more complete shell. Similar surface characteristics can be observed for CGB4 and CHGB. Based on the coating distribution, sample CGB1 and CGB2 were classified as partially coated. Samples CGB3, CGB4 and CHGB can be described as covered by a coating shell. Samples CGB2 and CGB3 possess an identical coating quantity (0.1%), at varying distribution (partial coating vs. coating shell). Samples CGB4 and CHGB possess identical coating quantity (0.2%) and distribution (coating shell) but differ in terms of core material (GB vs. HGB).

Table 1: Average cocoa butter content (% w/w) with standard deviation (bracketed values), sample classification according to coating type and contact angle ($\theta_{a,i}$) with 95%-Confidence interval (bracketed values) for uncoated (HGB, GB) and coated (CGB1 - CGB4, CHGB) beads.

Sample	Cocoa butter (% w/w)	Coating type	$\theta_{a,i}$ (°)
HGB	0.0 (0.01)	Uncoated	43 (4)
GB	0.0 (0.02)	Uncoated	54 (3)
CGB1	< 0.1 (0.02)[a]	Partial coating	65 (4)
CGB2	0.1 (0.02)	Partial coating	70 (4)
CGB3	0.1 (0.02)	Coating shell	75 (3)
CGB4	0.2 (0.02)	Coating shell	73 (4)
CHGB	0.2 (0.03)	Coating shell	56 (4)

[a]Classified as < 0.1% based on measurement accuracy (experimental value: 0.03%)

Average contact angles are included in **Table 1**. The average contact angle of 54°, determined for GB, decreased to 43° (HGB) as a result of storage in HCl. Surface contamination is known

to alter contact angles between water and glass [39] and can explain the comparably high contact angle of GB and the increase of wettability after acid treatment.

An apparent contact angle of 108° (± 1°) was determined for pure cocoa butter. Accordingly, all coated beads possessed higher contact angles than the respective core materials. Even minor quantities of distributed coating material (CGB1) were sufficient to increase the contact angle significantly. The higher contact angle of pure cocoa butter in comparison to the ones of coated samples, suggests that the core material impacts sample wettability. Consequently, uncoated areas must be present for all samples, e.g. in the form of cracks in a coating shell. It must be considered that cocoa butter wettability can vary depending on the underlying crystal form, which, in turn, is influenced by the thermal history [40]. Moreover, the contact angle of pure cocoa butter was measured on a tablet of compressed cocoa butter powder and could be affected by tablet porosity. The wettability of coated areas on the particle surface might, therefore, differ from the one of pure cocoa butter and even a complete coating shell might not result in a contact angle of 108°.

Neither varying coating distribution at identical quantity (CGB2, CGB3) nor an increased coating quantity (CGB4) led to significant differences between contact angles. Hence, under the conditions explored, contact line pinning on a partially coated surface has the same effect as the presence of a coating shell. The impact of coating on wettability is less pronounced if HGB are used as core material. Even though coating quantity and distribution are comparable, the average contact angle of CHGB is lower than the one of CGB4. This indicates the existence of uncoated areas which enable intensified liquid spreading on the hydrophilic base and hence reduce contact angles. These findings highlight the importance of wettability contrasts for contact angles.

3.2 Effect of surface composition and wettability contrast on particle floating

Floating behaviour was examined for all samples to assess the effect of coating type on particle attachment to the air-water interface. Buoyancy effects are insufficient to enable particle floating for the system considered here ($\rho_s > \rho_l > \rho_a$). Hence, the capillary force determines if a particle is retained at the air-liquid interface or sinks [8]. All samples were able to float. However, the particles took up varying floating positions, depending on their surface properties. Immersion depth at 1 s floating time, referred to as initial floating position, is shown along with average contact angles in **Figure 4**. Liquid properties were kept constant during floating experiments. The minor coating quantities are not sufficient to alter particle density or size to an extend relevant for floating. For instance, a uniform distribution of 0.2% cocoa butter (ρ_s = 971– 989 kg/m^3 [41]) on a glass sphere ($\rho_s \approx$ 2500 kg/m^3 [38]) of 678 µm diameter (d_{50}) would result in a coating thickness of 0.6 µm and a decrease of solid density by 0.3%. Such changes alter the particle immersion depth by a maximum of 1 µm, as verified by theoretical calculations (based on Eqs. 1 – 3, 13, 14 and measured contact angles). Wettability is therefore the main factor that leads to variation of floating behaviour between the samples. In conformity with this, the initial floating position tends to decrease with increasing contact angle.

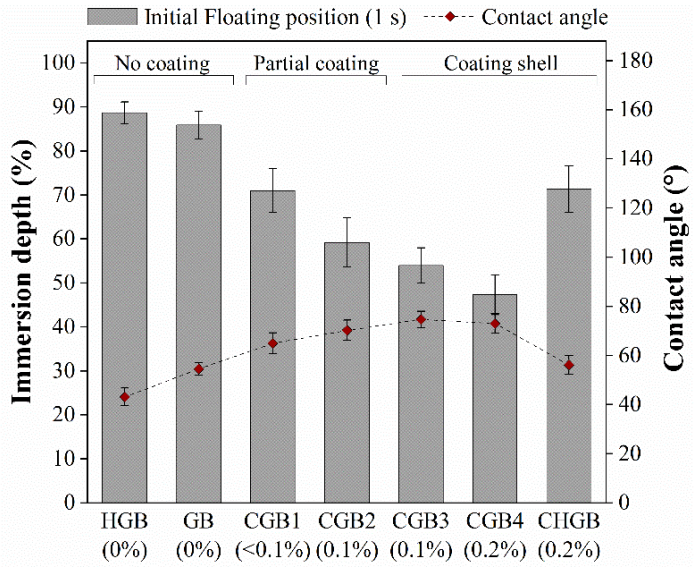

Figure 4: Immersion depth (%) determined at a floating time of 1 s (Initial floating position) and average contact angles. Error bars represent 95%-Confidence intervals.

HGB and GB took up a comparable initial floating position even though contact angles differed significantly. It is conceivable that impurities/chemical heterogeneities on the surface of GB are not sufficient to form strong contact line pinning points during floating, as gravity force counteracts pinning. For small sessile drops (drop diameter < capillary length), in contrast, gravity force is negligible and the effect of surface impurities on contact line pinning, and hence contact angles is more pronounced. It must be considered that the floating position can also be influenced by the experimental procedure (e.g. introduction of kinetic energy during particle positioning).

Partial coating with cocoa butter quantities below 0.1% (CGB1) decreased the immersion depth, in comparison to uncoated beads, significantly. Increasing coating quantity and/or surface coverage enhanced floating further, which can be explained by the reduction of coating-free areas. Using HGB as core material increased the immersion depth considerably, even if coating distribution and quantity were equivalent (CHGB vs CGB4). This demonstrates the importance of wettability contrasts. The increased immersion depth of CHGB is in agreement with the decreased contact angle. If measured contact angles were the only factor considered, the floating position of CHGB and GB, which differs by 15% (**Figure 4**), would have been expected to be similar. In general, measured contact angles were not suitable to indicate the floating behaviour of particles with heterogeneous surface composition. For instance, samples CGB2 and CGB4 possessed similar contact angles of 70° and 73°, but initial immersion depths of 59% and 47%, respectively. The comparison of sample CGB2 and CGB3 (identical coating quantity) illustrates that an increased surface coverage enhances floating, even though contact angles do not differ significantly.

Experimentally determined particle immersion depths are shown as a function of time for uncoated, partially coated and fully coated samples in **Figure 5a - c**. Exemplary images, depicting the immersed part of floating beads are included.

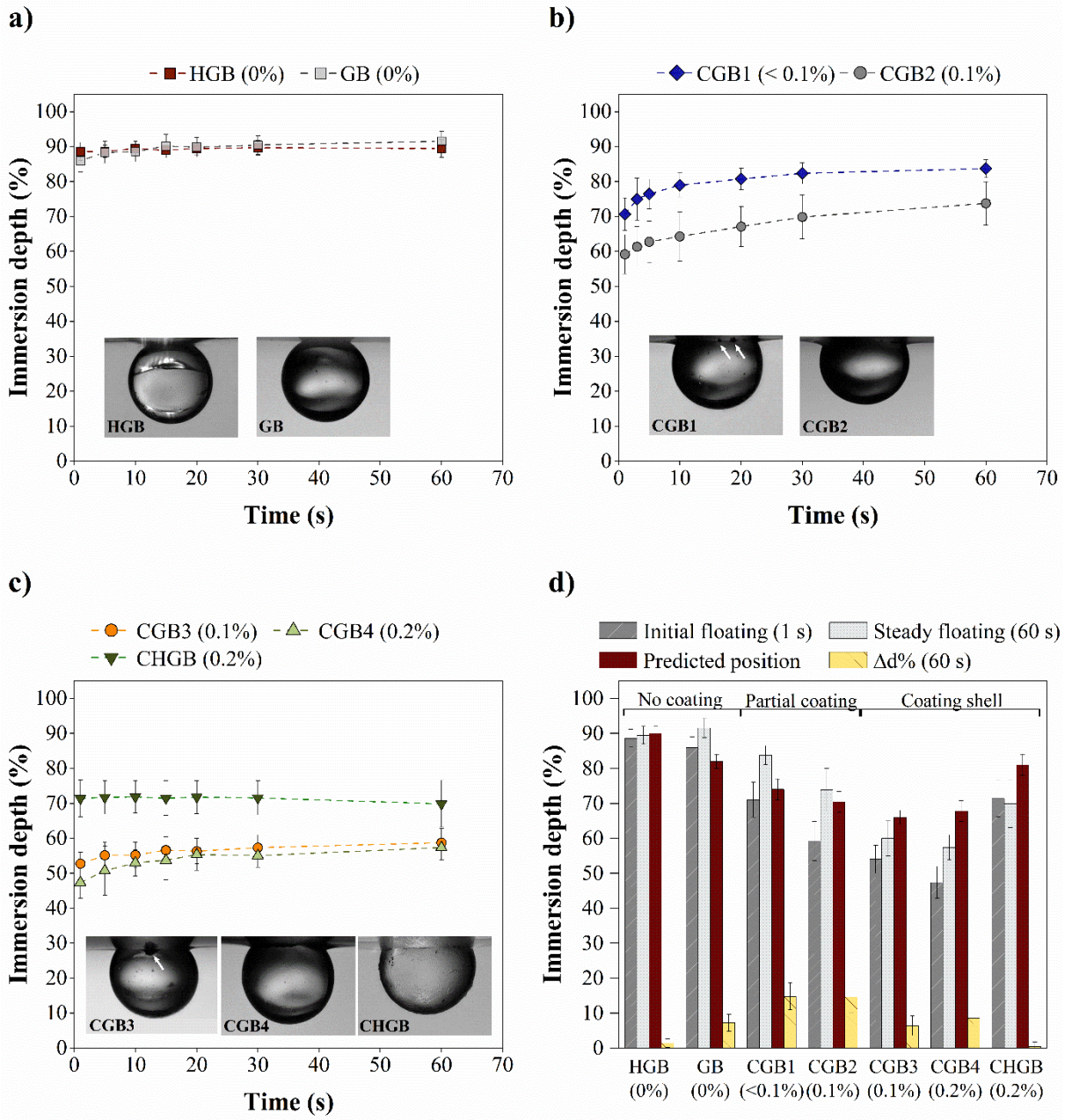

Figure 5: Average experimentally determined immersion depth (%) over time with exemplary images floating beads for a) Uncoated beads: HGB, GB; b) Partially coated beads: CGB1, CGB2; c) Beads comprising a Coating shell: CGB3, CGB4, CHGB. d) Comparison of average Initial floating position, Steady floating position, Predicted (Eqs. 1 – 3, 13, 14) immersion depth and average difference between initial and steady floating position (Δd% (60 s)). Error bars represent 95%-Confidence interval. Error bars of predicted values derive from experimentally observed contact angle variation considered for modelling. Arrows in inset images highlight contact line pinning and deformation.

GB and all coated samples (except CHGB) experienced an increase of immersion depth before the floating position stabilised. Hence, floating comprised a dynamic and a steady stage. The duration of the initial dynamic phase varied between replicates but was typically completed within 60 s. Frequently, a slow, marginal increase of immersion depth (µm range) occurred over a longer period. This was not sufficiently pronounced to affect *d*% values significantly. A comparison of average initial floating position (1 s), steady-state floating position (60 s), the difference between both values (Δd% (60 s)), as well as predicted (Eqs. 1 – 3, 13, 14) immersion depths off all samples is provided in **Figure 5d**. Since predicted values are calculated based on constant solid and liquid properties, no time dependency exists.

HGB are characterised by a stable floating position, which is accurately predicted (**Figure 5a/d**). This behaviour can be explained by the homogeneous surface chemistry, i.e. the constant surface wettability (neglecting ubiquitous variations leading to contact angle hysteresis). For a floating particle, this leads to a constant contact angle along the three-phase contact line and a uniform meniscus depression; a state which is in line with the schematic representation depicted in **Figure 1**. The immersion depth of GB increased by an average of 7% over a period of 60 s. The initial floating position of GB lies within the range of predicted values. The discrepancy between predicted and experimental values increases over time, resulting in an underestimation of actual (observed) immersion depth. Similar observations were made for sample CGB1. The increased surface coverage of sample CGB2 initially results in an immersion depth that is lower than theoretically expected.

Dynamic floating behaviour and discrepancies between experimental and predicted values can be explained by the heterogeneous surface composition. As the three-phase contact line encounters areas of varying wettability (coating spots), the contact line is pinned at defects and pronounced contact angle variations can be present. Each coating spot (or comparable surface defect/impurity) presents an energy barrier and results in contact line pinning and deformation (as indicated on the inset images in **Figure 5b/c**) if pronounced sufficiently. Such observations

were made during droplet spreading on patterned surfaces. Triple lines have been demonstrated to be stably pinned at localised defects but move and overcome pinning points if a sufficient outer force is applied (e.g. sliding drop, increase of droplet volume) [21, 23]. Pinning/depinning transitions of the contact line at hydrophobic fractions can also reduce a droplet's sliding velocity in comparison to a homogeneous surface [23]. Comparable to this, the observed dynamic floating phase can be described as a continuous pinning and depinning process. Beads are trapped initially but pinning points are gradually overcome until a sufficient number (and/or size) of pinning points is reached, so that the provided pinning force, along with the acting buoyancy force, balances the downward acting gravity force. Differences between experimental and predicted immersion depth most likely originate from contact angle values included in the model, as the impact of chemical heterogeneities/weak pinning points on contact angles and floating position (additional effect of gravity force) is differently pronounced.

Floating of samples CGB3 and CGB4 (coating shell) also comprises a dynamic phase (**Figure 5c**). However, average $\Delta d\%(60\ s)$ values are reduced in comparison to partially coated samples (**Figure 5d**), which can be explained by the increased surface coverage. Changes of immersion depth are absent for sample CHGB, even though surface heterogeneities (exposed core material) are present, as indicated by the reduced contact angle and the increased immersion depth compared to other coated samples. It is conceivable that the high wettability contrast between core and coating material accelerates the pinning/depinning process, as the contact line has an increased affinity to proceed towards the hydrophilic surface areas. As a consequence, the steady floating position is reached fast. Enhanced droplet spreading on hydrophilic regions of surfaces with alternating wettability has been reported previously [22]. Contact line progression can be accelerated on the hydrophilic section and decelerated on the hydrophobic section of a patterned surface [42]. It must also be considered that the coating characteristics of CHGB could deviate as a different coating technique was applied. This might affect floating

additionally. To which extent the height of a wettability contrast affects floating kinetics can, therefore, not be conclusively answered in the scope of this study.

Different to previous observations, predicted values underestimate the ability to float for samples comprising a coating shell (**Figure 5d**). This could be explained by strong contact line pinning at sharp edges (e.g. formed by cracks in the coating shell) and/or at surface roughness (generated by coating material). Such surface properties can increase contact angles locally and counteract depinning [26]. These local phenomena are not necessarily reflected by contact angle values, as small sessile drops only represent a limited surface fraction. In this case, implying a constant sessile drop contact angle for model predictions results in an underestimation of particle floating. Details concerning the limitation of sessile drop contact angles to reflect the properties of particles with heterogeneous surface characteristics (and hence to predict floating behaviour) are given in Section 3.4.

3.3 Effect of surface composition on forces acting during particle immersion

To assess magnitude and manner of contact line pinning, forces acting during immersion of individual beads were determined using force tensiometry. Exemplary force-position curves, recorded for individual beads of each sample are shown in **Figure 6**. Measured forces correspond to the sum of buoyancy and capillary force. Upon contact with water, the meniscus is concave and the recorded force is acting downward (positive value range). Continuous particle immersion results in a decrease of downward acting force. The force is upwards directed (negative value range) once the meniscus is convex. The immersion depth at which the interface curvature changes from concave to convex (zero force) depends on the contact angle [31].

In line with their homogeneous surface properties, force-position curves of HGB beads possess a smooth progression. Forces acting upon immersion of GB and partially coated beads (CGB1, CGB2) are subject to higher variations. Whilst the contact line is pinned at a defect (e.g. a

coating spot), and the bead is submerged further, the proportion of upward acting forces continuously increases until the contact line overcomes the pinning point and jumps forward (depinning). The stronger the contact line is pinned, the higher the abrupt force changes during pinning/depinning. Pronounced peaks were observed for samples CGB3 and CGB4 (highlighted by arrows) corresponding to force changes of 0.004 mN and 0.003 mN, respectively. This observation is in line with the suggested strong pinning at e.g. defects/cracks in the coating shell or surface roughness. The progression of the force-position curves supports the previously proposed type and extent of contact line pinning during floating.

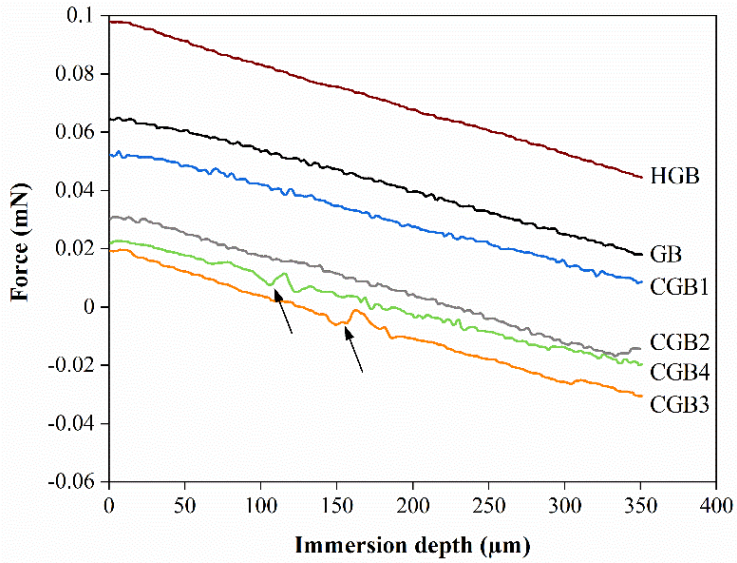

Figure 6: Exemplary force-position curves of uncoated beads (HGB, GB), partially coated beads (CGB1, CGB2), and beads comprising a coating shell (CGB3, CGB4). Arrows indicate intensive contact line pinning/depinning.

Averaged experimentally determined and theoretically predicted forces are plotted as a function of immersion depth (%) for uncoated, partially coated and fully coated samples in **Figure 7a** – **c**. Acting gravity force was calculated (Eq. 1) and included in the graphs to identify the immersion depth corresponding to the force balance (intersection of the curves). While local pinning effects are obscured by averaged values, general progression and differences between the samples are visible. The vertical shift of the curves shows that a coating shell provides

higher resistance against contact line movement than a partial coating. At an immersion depth of 50%, HGB, GB and CGB1 beads are still subject to downward acting (positive) forces. Due to the increased surface hydrophobicity of samples CGB2 – CGB4, the inflexion point (Force = 0 mN), at which upward acting forces (negative) prevail downward acting forces, is reached at lower immersion depths of 40% (CGB2), 34% (CGB3) and 28% (CGB4).

Forces measured during immersion of HGB and GB lie within the range of model predictions (**Figure 7a**). For HGB, the recorded force tends to be underestimated by calculated values. This deviation might be explained by variation of surface hydrophilicity during measurements of contact angles (considered for force calculation, Eq. 3) and force-position curves. For instance, differences in storage times after HCl treatment of glass slides have been found to affect measured contact angles (data not shown). Overall, it can be concluded that force-position curves and theoretical models (see **Figure 5d**) are suitable to reflect floating behaviour of beads with homogenous surface properties. For coated samples, measured forces are lower than theoretically expected (**Figure 7b/c**). Consequently, the force balance is reached at a lower immersion depth than predicted. A comparison of experimentally determined initial and steady floating position, predicted floating position (Eqs. 1 – 3, 13, 14) and floating position expected based on force position curves (immersion depth at which measured $F_b + F_c$ equals calculated F_g (Eq. 1) is provided in **Figure 7d**. Experimental immersion depths (particularly the steady floating position at 60 s) tend to be underestimated by force-position curves.

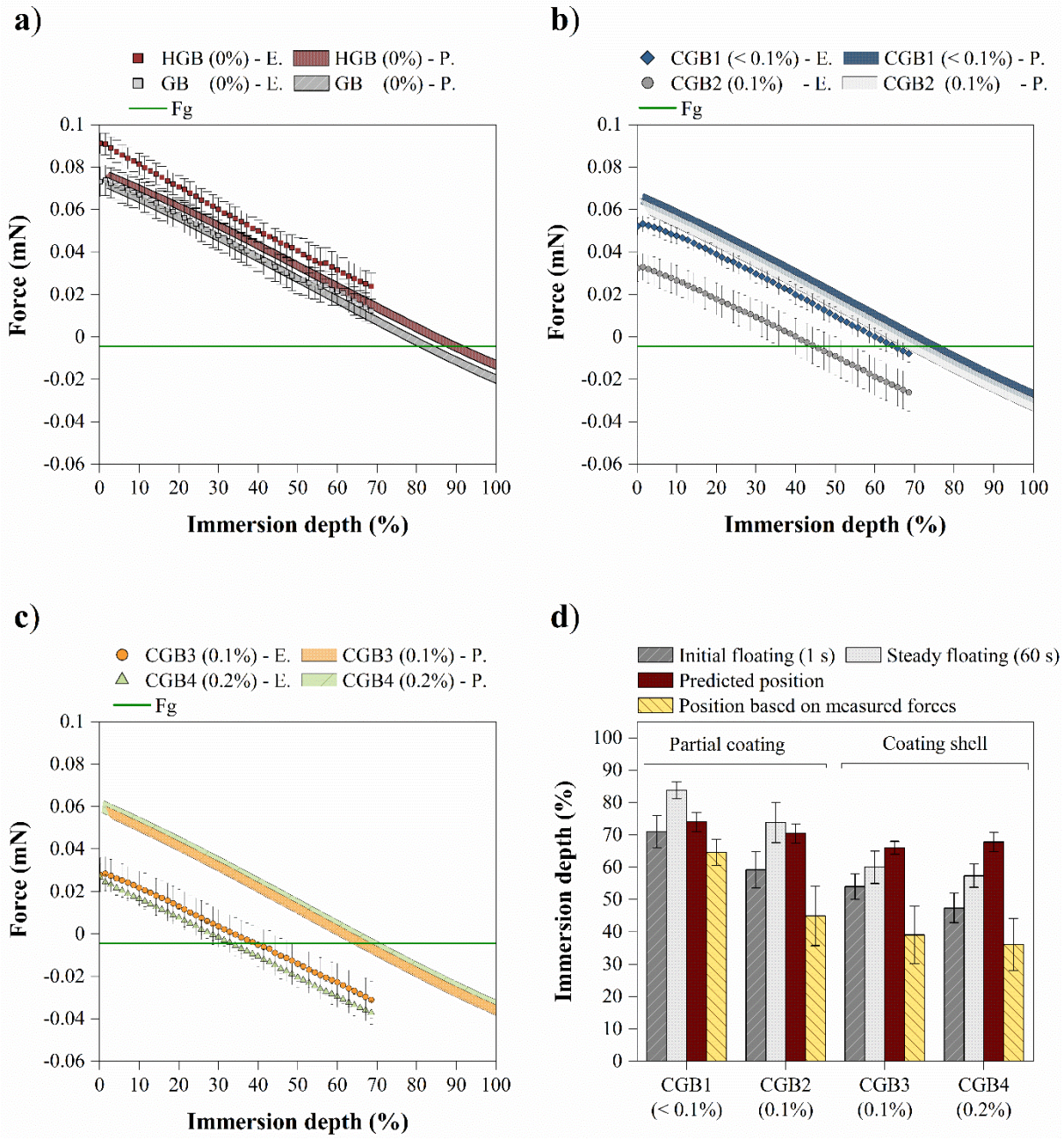

Figure 7: Average experimentally (E.) determined and predicted (P.) (Eqs. 1- 3, 13, 14) force-position curves of a) uncoated beads, b) partially coated beads, c) beads comprising a coating shell. Acting gravity force is shown to determine the force balance. For clarity, measured forces are shown in 10 µm steps. d) Comparison of average initial floating position, steady floating position, predicted position and floating position derived from measured forces. Error bars represent 95%-Confidence interval. The range of predicted values derives from experimentally observed contact angle variation (95%-Confidence interval) considered for modelling.

Different factors can contribute to the discrepancy between the experimentally determined floating position and the floating position expected based on measured force-position curves. The surface properties of beads can differ within a sample (i.e. beads can possess a different magnitude and form of pinning points), leading to a certain variation. Moreover, contact between beads and air-liquid interface is more controlled during tensiometric measurements. Even though particles were placed carefully on the interface during floating experiments, it cannot be excluded that kinetic energy was introduced, which can facilitate contact line movement across pinning points and hence increases the initial floating position. The particle size range considered for force measurements was more restricted (R_p = 350 ± 10 µm) than the one during floating experiments (R_p = 350 ± 50 µm) to provide one defined particle size value for the calculation of theoretical force-position curves. Since larger particle sizes increase gravity force, the force balance is reached at a higher immersion depth. However, additional force measurements conducted for beads with R_p = 400 ± 10 µm (data not shown), increased the expected floating position by a maximum of 2%. At the same time, increased gravity force could facilitate contact line depinning during floating. However, no trend between particle size (in the considered range) and increase of immersion depth over time (Δd% (60s)) was observed. The gradual increase of immersion depth during floating could also be facilitated by condensation on the non-immersed particle surface. Condensation alters the interfacial free energy of a solid-gas interface and consequently increases surface wettability [43]. The associated decrease of contact angles has been demonstrated previously [43, 44]. Immediate and intensive condensation on the non-wetted sphere surface was observed during floating of all samples and is shown for HGB and CGB1 in **Figure 8**. During tensiometric measurements, the particles were immersed 500 µm (approx. 74%) at a velocity of 1000 µm/min, whereas the immersion depth increased by a maximum of 15% (CGB1) within 60 sec during floating. The experimental conditions of particle floating (prolonged exposure to saturated water vapour), should, therefore, result in more pronounced condensation. Consequently, strong pinning

points, which significantly increase measured forces, might be overcome during floating. The increase of immersion depth in top view images can be seen from the reduction of contact line length (indicated by dashed lines). As the immersion depth of HGB is constant over time, condensation in front of the contact line does not seem to have any effect on floating of homogeneous beads. Note that the decrease of contact line length observed for CGB1 at a floating time of 5 min does not change the percentage immersion depth significantly.

The observation that forces, measured on heterogeneous particles, are consistently lower than theoretically predicted **Figure 7b/c**, can be explained by the calculation of acting capillary force (Eq. 3) based on experimentally determined sessile drop contact angles. The limited surface area covered by a sessile drop is not necessarily suitable to reflect the wetting properties of particles with heterogeneous surface composition, as discussed in Section 3.4.

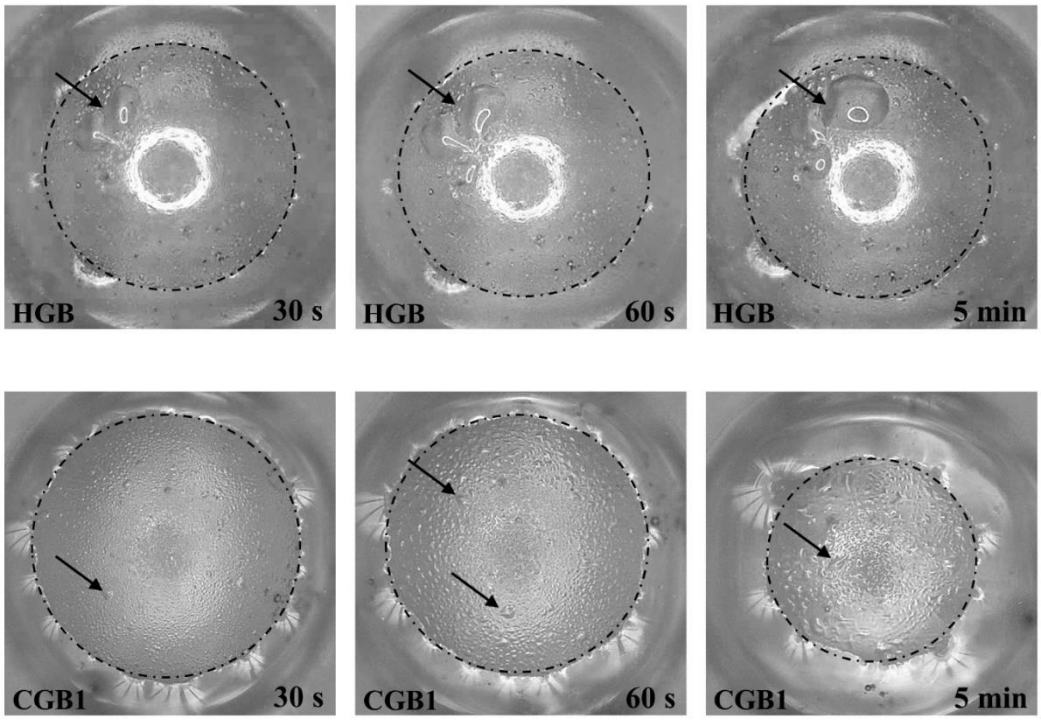

Figure 8: Exemplary top view images of floating HGB and CGB1 beads (recorded at 200 x magnification) showing condensation on the non-immersed particle surface over time. For clarity, the three-phase contact line is indicated by a dashed line. Condensation was observed across the entire non-immersed particle surface, the formation of larger droplets is highlighted by arrows.

3.4 Limitation of sessile drop contact angles to reflect heterogeneous surface properties

Uncertainties of theoretical predictions for particles with heterogeneous surface properties can arise due to the assumption of a constant sessile drop contact angle. Firstly, weak pinning points can be sufficient to pin small sessile drops but are overcome during floating and therefore result in an overestimation of floating behaviour. Secondly, the limited surface area represented by sessile drops can conceal contact line pinning at local defects, which leads to a lower immersion depth than theoretically expected. To illustrate this effect, force-position curves were determined for glass beads with defined surface coating. **Figure 9a** depicts forces measured during immersion of a top-coated bead and a bead comprising a coating pattern. The sphere pole of the former is covered by a coating spot until a particle height of 158 ± 49 µm. The patterned coated sample comprises an uncoated sphere apex and four separated coating spots beginning at 310, 366, 431 and 721 µm distance from the sphere apex and reaching until a distance of 2410, 2146, 2613 and 3030 µm below the sphere apex (compare inset images in **Figure 9a**).

The initial force, measured upon immersion, is lower for a bead with patterned coating in comparison to a top-coated bead. The distributed coating spots have an immediate effect on acting forces, even though the top of the sphere is uncoated. This can be explained by the meniscus jump-in. The same effect conceals the presence of the coating spot on a top-coated sample. The contact line "jumps" over the coating spot and the recorded force is comparable to the one of a completely uncoated bead, as can be seen in **Figure 9b**. The step-wise increase of acting forces observed for the patterned coated bead (highlighted by arrows) is caused by depinning from each coating spot. Subsequent to this, the contact line proceeds on the coating-free bead surface and the measured force corresponds to the one of an uncoated bead (**Figure 9b**). The effect of wettability contrast is also shown by the comparison with forces acting on a fully coated bead (**Figure 9b**). Prior to depinning, the force acting on the patterned coated bead lies between the one of an uncoated and a fully coated bead.

While the observed force progression is conclusive, sessile drop contact angles, measured on the sphere apex would have led to different expectations. A sessile drop, placed on the coating-free apex of a patterned coated bead, would insinuate the wettability of an uncoated bead. The overall effect of coating spots on acting forces as well as contact line pinning at coating spots experienced throughout immersion is not reflected. Theoretical predictions would correspond to the ones of uncoated beads, included in **Figure 9b**. A sessile drop, located on the pole of a top-coated sample, in contrast, would imply the wettability of a fully coated bead.

These model experiments illustrate in a simple way how the use of a sessile drop contact angle can result in a misleading representation of wetting characteristics and consequently an incorrect estimation of acting forces and particle floating behaviour.

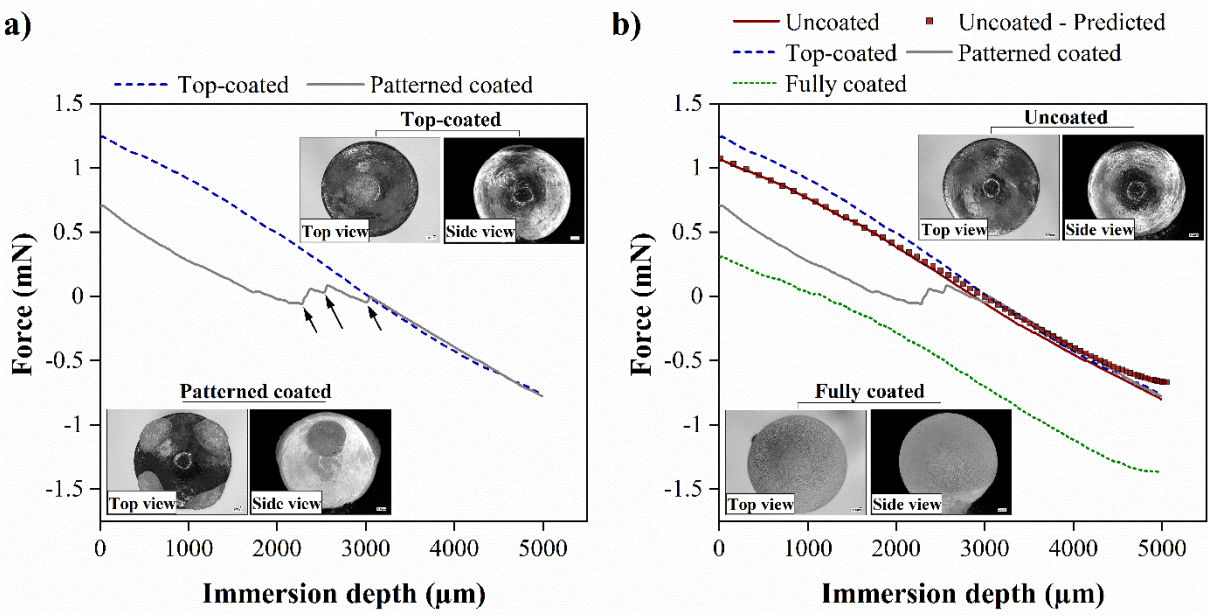

Figure 9: Force-position curves measured for a) a top-coated and a patterned coated glass bead (arrows indicate contact line depinning) and b) an uncoated, a top-coated, a patterned coated and a fully coated glass bead. Theoretically predicted forces for the case of an uncoated bead are shown additionally.

4 Conclusions

In this work, the effect of surface heterogeneity, in the form of distributed hydrophobic coating material (partial coating) and as defects in a coating shell, on floating of glass beads was investigated. This approach was chosen as surfaces of food particles are frequently characterised by the presence of hydrophobic areas, such as free fat in dairy powders. The study was conducted to enhance the understanding of particle floating which plays an important role in reconstitution performance.

Surface heterogeneities significantly influence particle immersion depth and prolong the time to reach a steady floating position. The observed dynamic phase is explained by a continuous process of contact line pinning and depinning. Even minor quantities (< 0.1%) of distributed hydrophobic defects can inflict wettability degradation, affect particle floating and can hence deteriorate powder reconstitution.

Established models are accurate to describe acting forces and resulting floating position for particles with homogeneous surface properties but lack applicability if surface heterogeneities are present. The results presented in this paper show that an important source of error in established models is the assumption of a constant (sessile drop) contact angle. Force-position curves can help to understand floating of particles with heterogeneous surface composition, as the resistance against contact line progression as well as specific phenomena such as contact line pinning at defects are displayed. It was furthermore proven that intensive condensation on the non-immersed particle surface occurs during floating. Even though water adsorption can increase wettability in front of the three-phase contact line, it was shown that this phenomenon does not affect floating of glass beads. It has also been found that the height of the wettability contrast might play an important role for floating position and kinetics and requires more investigation in the future. It is also suggested to examine the effect of heterogeneous surface wettability on floating for particles of varying size and density. To further understand the

behaviour of real powders at interfaces, particle dissolution, a common feature of food powders, but neglected in available floating studies, should also be considered.

Notation

a	Sessile drop contact line cord/2
d	Immersion depth
$d\%$	Percentage of immersion depth (percentage of particle diameter, immersed in water)
F_b	Buoyancy force
F_c	Capillary force
F_g	Gravity force
g	Accerleration due to gravity
h	Coordinate of the meniscus depth
H	Meniscus depth at the three-phase contact line
K_0	Modified Bessel function of the second kind and zero order
K_1	Modified Bessel function of the second kind and first order
L	Capillary length
r	Radial meniscus coordinate
Rp	Particle radius
V_p	Particle volume

Greek symbols

α	Immersion angle
β	Meniscus slope angle
γ	Liquid surface tension
θ	Contact angle
θ_a	Apparent contact angle
$\theta_{a,i}$	Intrinsic contact angle
ρ_a	Air density
ρ_l	Liquid density
ρ_s	Solid density

Funding

This work was supported by the Nestec Ltd., Vevey, Switzerland.

References

[1] L. Forny, A. Marabi, S. Palzer, Wetting, disintegration and dissolution of agglomerated water soluble powders, Powder Technol. 206 (2011) 72-78.

[2] J. Dupas, V. Girard, L. Forny, Reconstitution Properties of Sucrose and Maltodextrins, Langmuir 33 (2017) 988-995.

[3] J. Dupas, L. Forny, M. Ramaioli, Powder wettability at a static air–water interface, J. Colloid Interface Sci. 448 (2015) 51-56.

[4] D. Angelopoulou, V. Meunier, L. Forny, G. Niederreiter, S. Palzer, A.D. Salman, Particle surface design for enhanced reconstitution of fat-based food powders, Powder Technol. 393 (2021) 397-404.

[5] C.W. Nutt, Froth flotation: The adhesion of solid particles to flat interfaces and bubbles, Chem. Eng. Sci. 12 (1960) 133-141.

[6] C. Huh, L.E. Scriven, Shapes of axisymmetric fluid interfaces of unbounded extent, J. Colloid Interface Sci. 30 (1969) 323-337.

[7] C. Huh, S.G. Mason, The flotation of axisymmetric particles at horizontal liquid interfaces, J. Colloid Interface Sci. 47 (1974) 271-289.

[8] A.V. Rapacchietta, A.W. Neumann, S.N. Omenyi, Force and free-energy analyses of small particles at fluid interfaces: I. Cylinders, J. Colloid Interface Sci. 59 (1977) 541 - 554.

[9] A.V. Rapacchietta, A.W. Neumann, Force and free- energy analyses of small particles at fluid interfaces: II. Spheres, J. Colloid Interface Sci. 59 (1977) 555-567.

[10] I.B. Ivanov, P.A. Kralchevsky, A.D. Nikolov, Film and line tension effects on the attachment of particles to an interface: I. Conditions for mechanical equilibrium of fluid and solid particles at a fluid interface, J. Colloid Interface Sci. 112 (1986) 97-107.

[11] D.-X. Feng, A.V. Nguyen, A novel quantitative analysis of the local deformation of the air-water surface by a floating sphere, Colloids Surf. A: Physicochem. Eng. Asp. 504 (2016) 407-413.

[12] D.-X. Feng, A.V. Nguyen, Contact angle variation on single floating spheres and its impact on the stability analysis of floating particles, Colloids Surf. A: Physicochem. Eng. Asp. 520 (2017) 442-447.

[13] J. Lee, The Static Profile for a Floating Particle, Colloids Interfaces 2 (2018) 18.

[14] C.W. Extrand, S.I. Moon, Using the Flotation of a Single Sphere to Measure and Model Capillary Forces, Langmuir 25 (2009) 6239-6244.

[15] X. Liu, X. Wang, Y. Liang, F. Zhou, Floating behavior of hydrophobic glass spheres, J. Colloid Interface Sci. 336 (2009) 743-749.

[16] D.-X. Feng, A.V. Nguyen, Effect of contact angle and contact angle hysteresis on the floatability of spheres at the air- water interface, Adv. Colloid Interface Sci. 248 (2017) 69-84.

[17] A.V. Nguyen, H.J. Schulze, Colloidal Science of Flotation, Taylor & Francis Group, Boca Raton, 2003.

[18] D. Vella, D.G. Lee, H.Y. Kim, The load supported by small floating objects, Langmuir 22 (2006) 5979-5981.

[19] A.V. Nguyen, Empirical Equations for Meniscus Depression by Particle Attachment, J. Colloid Interface Sci. 249 (2002) 147-151.

[20] J.F. Joanny, P.G. de Gennes, A model for contact angle hysteresis, J. Chem. Phys. 81 (1984) 552-562.

[21] S. Suzuki, A. Nakajima, K. Tanaka, M. Sakai, A. Hashimoto, N. Yoshida, Y. Kameshima, K. Okada, Sliding behavior of water droplets on line-patterned hydrophobic surfaces, Appl. Surf. Sci. 254 (2008) 1797-1805.

[22] H.P. Jansen, O. Bliznyuk, E.S. Kooij, B. Poelsema, H.J.W. Zandvliet, Simulating anisotropic droplet shapes on chemically striped patterned surfaces, Langmuir 28 (2012) 499-505.

[23] S. Varagnolo, D. Ferraro, P. Fantinel, M. Pierno, G. Mistura, G. Amati, L. Biferale, M. Sbragaglia, Stick-slip sliding of water drops on chemically heterogeneous surfaces, Phys. Rev. Lett. 111 (2013) 066101-066101.

[24] S. Neuhaus, N.D. Spencer, C. Padeste, Anisotropic wetting of microstructured surfaces as a function of surface chemistry, ACS Appl. Mater. Interfaces 4 (2012) 123-130.

[25] J.F. Oliver, C. Huh, S.G. Mason, Resistance to spreading of liquids by sharp edges, J. Colloid Interface Sci. 59 (1977) 568-581.

[26] P. Singh, D.D. Joseph, Fluid dynamics of floating particles, J. Fluid Mech. 530 (2005) 31-80.

[27] J. Shang, M. Flury, D. Youjun, Force measurements between particles and the air-water interface: Implications for particle mobilization in unsaturated porous media, Water Resour. Res. 45 (2009) W06420-n/a.

[28] D.-X. Feng, A.V. Nguyen, How Does the Gibbs Inequality Condition Affect the Stability and Detachment of Floating Spheres from the Free Surface of Water?, Langmuir 32 (2016) 1988-1995.

[29] J. Ally, M. Kappl, H.-J. Butt, Adhesion of particles with sharp edges to air-liquid interfaces, Langmuir 28 (2012) 11042-11047.

[30] N. Chatterjee, S. Lapin, M. Flury, Capillary Forces between Sediment Particles and an Air–Water Interface, Environ. Sci. Technol. 46 (2012) 4411-4418.

[31] N. Chatterjee, M. Flury, Effect of particle shape on capillary forces acting on particles at the air-water interface, Langmuir 29 (2013) 7903-7911.

[32] M. Yekeler, U. Ulusoy, C. Hiçyılmaz, Effect of particle shape and roughness of talc mineral ground by different mills on the wettability and floatability, Powder technol. 140 (2004) 68-78.

[33] X. Wang, Q. Zhang, Role of surface roughness in the wettability, surface energy and flotation kinetics of calcite, Powder technol. 371 (2020) 55-63.

[34] E.H.J. Kim, X.D. Chen, D. Pearce, Surface characterization of four industrial spray- dried dairy powders in relation to chemical composition, structure and wetting property, Colloids Surf. B: Biointerfaces 26 (2002) 197-212.

[35] C. Gaiani, P. Boyanova, R. Hussain, I. Murrieta Pazos, M.C. Karam, J. Burgain, J. Scher, Morphological descriptors and colour as a tool to better understand rehydration properties of dairy powders, Int. Dairy J. 21 (2011) 462-469.

[36] C. Jacquot, J. Petit, F. Michaux, E. Chávez Montes, J. Dupas, V. Girard, A. Gianfrancesco, J. Scher, C. Gaiani, Cocoa powder surface composition during aging: A focus on fat, Powder technol. 292 (2016) 195-202.

[37] C.W. Extrand, S.I. Moon, Contact angles on spherical surfaces, Langmuir 24 (2008) 9470-9473.

[38] J.E. Shelby, Introduction to glass science and technology, 2nd ed. ed., Royal Society of Chemistry, Cambridge, 2005.

[39] S. Iglauer, A. Salamah, M. Sarmadivaleh, K. Liu, C. Phan, Contamination of silica surfaces: Impact on water–CO2–quartz and glass contact angle measurements, Int. J. Greenh. Gas Control 22 (2014) 325-328.

[40] S.K. Reinke, K. Hauf, J. Vieira, S. Heinrich, S. Palzer, Changes in contact angle providing evidence for surface alteration in multi-component solid foods, J. Phys. D: Appl. Phys. 48 (2015) 464001.

[41] R.W. Lencki, R.J. Craven, Negative Pressure Induced Cavity Formation During Cocoa Butter Crystallization, J. Am. Oil Chem. Soc. 90 (2013) 1-8.

[42] J. Léopoldès, D.G. Bucknall, Droplet Spreading on Microstriped Surfaces, J. Phys. Chem. B 109 (2005) 8973-8977.

[43] T. Furuta, M. Sakai, T. Isobe, A. Nakajima, Effect of Dew Condensation on the Wettability of Rough Hydrophobic Surfaces Coated with Two Different Silanes, Langmuir 26 (2010) 13305-13309.

[44] K.A. Wier, T.J. McCarthy, Condensation on Ultrahydrophobic Surfaces and Its Effect on Droplet Mobility: Ultrahydrophobic Surfaces Are Not Always Water Repellant, Langmuir 22 (2006) 2433-2436.